Available online at www.sciencedirect.com
SCIENCE DIRECT®
C. R. Physique 4 (2003) 993–1008
COMPTES RENDUS PHYSIQUE

Carbon nanotubes: state of the art and applications/Les nanotubes de carbone : état de l'art et applications

Mechanical properties of carbon nanotubes: theoretical predictions and experimental measurements

Rodney S. Ruoff [a,*], Dong Qian [b], Wing Kam Liu [a]

[a] *Department of Mechanical Engineering, Northwestern University, 2145 Sheridan Road, Evanston, IL 60208, USA*
[b] *Department of Mechanical, Industrial and Nuclear Engineering, University of Cincinnati, Cincinnati, OH 45221-0072, USA*

Presented by Guy Laval

Abstract

Mechanical properties of carbon nanotubes are discussed based on recent advances in both modeling and experiment. ***To cite this article: R.S. Ruoff et al., C. R. Physique 4 (2003).***
© 2003 Académie des sciences. Published by Elsevier SAS. All rights reserved.

Résumé

Propriétés mécaniques des nanotubes de carbone : prédictions théoriques et résultats expérimentaux. Les propriétés mécaniques des nanotubes de carbone sont discutées à la lumière des dernières avancées dans la modélisation et l'expérimentation. ***Pour citer cet article : R.S. Ruoff et al., C. R. Physique 4 (2003).***
© 2003 Académie des sciences. Published by Elsevier SAS. All rights reserved.

1. Introduction

Significant progress has been made in the area of nanoscale science and technology in the past decade. As one of the most interesting nanomaterials, carbon nanotubes (CNT) have received significant attention in terms of fundamental properties measurements and potential applications. This is largely due to the impressive physical properties as revealed from both theoretical and experimental studies. For example, the electrical properties of CNT may be tuned by mechanical deformation. Such properties are of great interest for applications such as sensors or smart materials. The study of these properties is multi-disciplinary and involves various branches of science and engineering.

Steady progress has been made in exploring the mechanical properties and potential applications of two types of CNTs: single-walled carbon nanotubes (SWCNT) and multi-walled carbon nanotubes (MWCNT). The measured specific tensile strength of a single layer of a multi-walled carbon nanotube can be as high as 100 times that of steel, and the graphene sheet (in-plane) is as stiff as diamond at low strain. These mechanical properties motivate further study of possible applications for lightweight and high strength materials. Composite materials reinforced by either SWCNT or MWCNT have been fabricated and significant enhancement in mechanical properties has been recently reported [1].

* Corresponding author.
E-mail addresses: r-ruoff@northwestern.edu (R. Ruoff), dong.qian@uc.edu (D. Qian), w-liu@northwestern.edu (W.K. Liu).

1631-0705/$ – see front matter © 2003 Académie des sciences. Published by Elsevier SAS. All rights reserved.
doi:10.1016/j.crhy.2003.08.001

2. Molecular structure

2.1. Structure of the bond

CNT is a cylindrical molecule composed of carbon atoms. A typical SWCNT structure is illustrated in Fig. 1. A major feature of the structure is the hexagon pattern that repeats itself periodically in space. As a result of the periodicity, each atom is bonded to three neighboring atoms. Such structure is mainly due to the process of sp^2 hybridization [2] during which one s-orbital and two p-orbitals combine to form three hybrid sp^2-orbitals at 120° to each other within a plane (shown in Fig. 2 for part of a graphene sheet). This covalent bond (referred to as the σ-bond) is a strong chemical bond and plays an important role in the impressive mechanical properties of CNT's. In addition, the out-of-plane bond (the π-bond) that is relatively weak contributes to the interaction between the layers in MWCNTs, and between SWCNT's in SWCNT bundles. Of course, the bonding is not purely sp^2 in nanotubes, as curving the graphene sheet into a tube re-hybridizes the σ and π orbitals, yielding an admixture.

2.2. Structures of single-walled carbon nanotube

As described above, the bonding in CNTs is similar, but not identical, to the graphene sheet. A widely used approach to identify the types of SWCNT is by reference to rolling up the graphene sheet. The key geometric parameter associated with this process is the roll-up vector $\boldsymbol{r}$, which can be expressed as the linear combination of the lattice basis ($\boldsymbol{a}$ and $\boldsymbol{b}$). Following the notation in [3–5] and Fig. 3, we have:

$$\boldsymbol{r} = n\boldsymbol{a} + m\boldsymbol{b}. \tag{1}$$

It is then possible to associate a particular integer pair (n, m) with each SWCNT. The relation between n and m also defines three categories of CNT:

$m = 0$, 'Zigzag',

$n = m$, 'Armchair',

other, 'Chiral'.

SWCNT can have either open ends or closed ends. Modeling suggests that for CNT to have stable closed ends, it has to be larger in diameter than the (5,5) and (9,0) tubes [3,5,6]. The shapes of the ends are not unique for CNTs with the same radius. For instance, a 'Bill'-like [7] or a semi-toroidal [8] end cap can occur. CNTs with open ends can be found in experimental observation, as reported in [8].

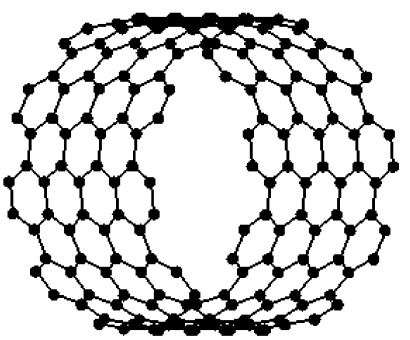

Fig. 1. Molecular structure of a section of (10, 10) CNT. Each node shown is a carbon atom and lines are the chemical bonds.

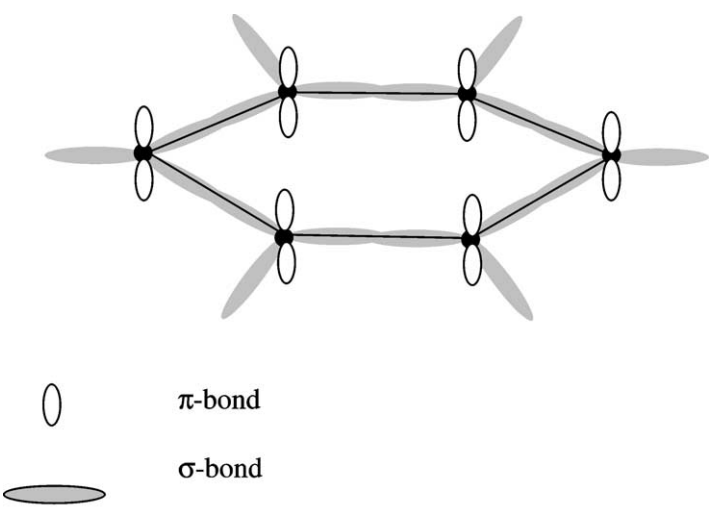

Fig. 2. Basic hexagonal bonding structure for one graphite layer (the 'graphene sheet'). Carbon nuclei shown as filled circle, out-of-plane π-bonds, and σ-bonds connect the C nuclei in-plane.

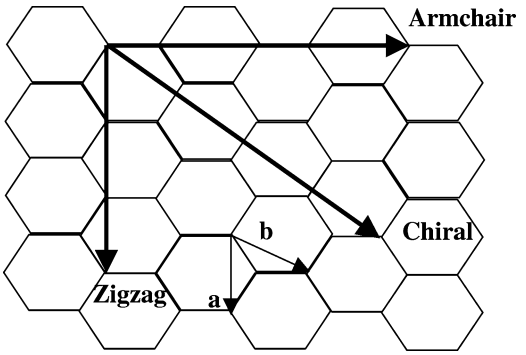

Fig. 3. Definition of roll-up vector as linear combinations of base vectors ***a*** and ***b***.

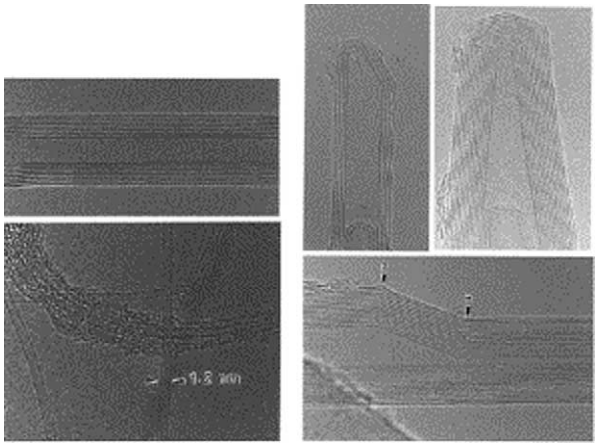

Fig. 4. Upper left: HRTEM (High resolution transmission electronic microscopy) image of an individual MWCNT. The parallel fringes have ∼0.34 nm separation between them and correspond to individual layers of the coaxial cylindrical geometry. Bottom left: HRTEM image showing isolated SWCNT as well as bundles of such tubes covered with amorphous carbon. The isolated tubes shown are approximately 1.2 nm in diameter. Top center: HRTEM image showing the tip structure of a closed MWCNT. The fringe (layer) separation is again 0.34 nm. Top right: the tip structure of a conical end. Bottom right: the image of a MWCNT showing the geometric changes due to the presence of five and seven membered rings (position indicated in the image by 'P' for pentagon (upper arrow) and 'H' for heptagon (lower arrow)) in the lattice. Note that the defects in all the neighboring shells are conformal (from [14], with the authors' permission, and permission of the IOP).

2.3. Structures of multi-walled carbon nanotubes

MWCNTs (shown in Fig. 4) are essentially nested CNT shells. The interlayer distance is ∼0.34 nm [9,10], close to that of graphite, 0.335 nm. The effect of the curvature on the interlayer distance was reported by Kiang et al. [11] who observed that the interlayer distance ranges from 0.342 to 0.375 nm, and that it is a function of the curvature and number of layers. Besides the nested shell model, experimental observation [10,12,13] also suggests that another candidate form of MWCNT is simply a 'cinnamon roll' – like structure.

3. Bonding models

3.1. Bonding potentials

Several empirical potentials are available that model the covalent bond in CNT. These atomistic models can be used to predict the mechanical properties. The existing empirical models can be categorized as follows.

3.1.1. Force field model

Examples include molecular mechanics force field #2 (MM2) and an improved version known as the MM3 force field, due to Allinger and co-workers [15,16]. A generic force field was also proposed by Mayo et al. [17]. Implementation of the model in molecular dynamics simulation can be found in the work of Guo et al. [18] and Tuzun et al. [19,20].

3.1.2. Bond order model

This model is proposed by Abell [21], in which he explored the universality in bonding of similar elements. Extension to the carbon system was made by Tersoff [22–25]. A significant further step was taken by Brenner [26], in which a bond order function was introduced; the main purpose was to describe the effect due to the formation and breakage of the C–C bond. Brenner's potential model has been used widely to explore the formation of fullerenes and their properties [27–30], indentation and friction at nanoscale [31–40], and energetics of nanotubes [29]. Recently, a second generation of the Brenner potential was proposed [41,42]; the potential is typically referred to as the *Tersoff–Brenner* potential.

3.1.3. Semi-empirical model

This model was proposed by Pettifor and Oleinik [43,44] and is derived based on a tight-binding approach. Application of this model to hydrocarbon systems can be found in [43].

3.2. Interlayer potentials

The Lennard–Jones (LJ) potential energy has been widely used in treating the interlayer interaction. For example, Girifalco and Lad [45,46] provided the following form for the carbon–carbon system:

$$\phi_i = \frac{A}{\sigma^6}\left[\frac{1}{2}y_0^6\frac{1}{(r_i/\sigma)^{12}} - \frac{1}{(r_i/\sigma)^6}\right]. \tag{2}$$

In (2), σ is the bond length, y_0 is a dimensionless constant, and r_i is the distance between the i-th atom pair. The model parameters with the corresponding sources of reference are given in Table 1. The universality of the LJ types has been studied by Girifalco et al. [47].

A different functional form of the interlayer potential was proposed by Wang et al. [48] based on the local density approximation (LDA) method:

$$U(r) = D_e\left\lfloor\left(1 - e^{-\beta(r-r_e)}\right)^2 - 1\right\rfloor + E_r e^{-\beta' r}, \tag{3}$$

where $D_e = 6.50 \times 10^{-3}$ eV is the equilibrium binding energy, $E_r = 6.94 \times 10^{-3}$ eV is the hard-core repulsion energy, $r_e = 4.05$ Å is the equilibrium distance between two carbon atoms, $\beta = 1.00$ Å^{-1} and $\beta' = 4.00$ Å^{-1}.

Qian et al. [49] have computed the equation of state (EOS) for graphite and compared the results with existing experimental data [50] and the ab initio calculation by Boetgger [51]; they concluded that the LDA model corrects the overly-repulsive LJ model in the high pressure region (interlayer distance <3.3 Å). However, how the LDA model performs for interlayer distance under 0.26 nm is unknown. A challenge for the future is experimental interrogation, and also modeling, of the transition 'through' the repulsive region into the region on the potential energy surface where new bonds have been formed.

Kolmogorov and Crespi [52] developed a new *registry-dependent graphite potential*. This potential includes the effects due to the exponential atomic-core repulsion and the interlayer delocalization of π orbitals in addition to the normal two-body van der Waals attraction. In terms of the functional dependence, the potential is not only a function of the inter-layer distance, it also depends on the relative position of the two layers (the registry between layers). Extension of its use to relaxed MWCNT [52] and collapsed MWCNT [53] systems has been made. It is not likely that this potential can be used, in its present form, for systems that do not have high symmetry. The further development of a general model of interlayer interaction is essential for understanding nanoscale interlayer energetics and tribology.

Table 1
Model parameters for LJ potential

Parameter sources	A (J·m^6)	σ (Å)	y_0
LJ1 [45]	24.3×10^{-79}	1.42	2.7
LJ2 [46]	32×10^{-79}	1.42	2.742

4. Elastic properties of CNT

4.1. Young's modulus

By assuming CNT as a structural member, the elastic properties of CNT can be obtained from experimental observations. Typical examples of structural member include bar, beam, and shell models. The bar model has been used in the experiment by Lourie and Wagner [54], in which the compressive response was measured using micro-Raman spectroscopy. They reported Young's modulus of 2.8–3.6 TPa, for SWCNT and 1.7–2.4 TPa for MWCNT. Direct tensile loading tests of SWCNT [55] and MWCNT [56] have been performed by Yu et al. The Young's modulus obtained ranges from 320 to 1470 GPa (mean: 1002 GPa) for SWCNT and from 270 to 950 GPa for MWCNT. The stress–strain curves obtained for these two types of CNT are shown below (Figs. 5 and 6). Note that the stress and strain correspond to the definition of engineering stress and strain, and the stress is evaluated by assuming an equivalent thickness of 0.34 nm for each layer of loaded CNT.

A cantilevered beam model has been used in the experiment by Wong et al. [57] in which individual MWCNT were bent using an atomic force microscope tip. By fitting the measured static response to the analytical solution for a cantilevered beam, a Young's modulus of 1.28 ± 0.59 TPa was obtained. The simply-supported beam model was used by Salvetat et al. [58, 59] to model the deflections of individual MWCNTs and of different-sized SWCNT ropes; a Young's modulus of $\sim$1 TPa for MWCNTs grown by arc discharge was reported, whereas CNT grown by the catalytic decomposition of hydrocarbons, however, had a modulus 1–2 order of magnitude smaller. The shear modulus for SWCNTs was also reported.

Treacy et al. [60] were first to report fitting Young's modulus of MWCNT to experimental data. Their work was based on analysis of thermal vibration of MWCNT, modeled as a continuous beam. For a total of 11 MWCNT's Young's modulus

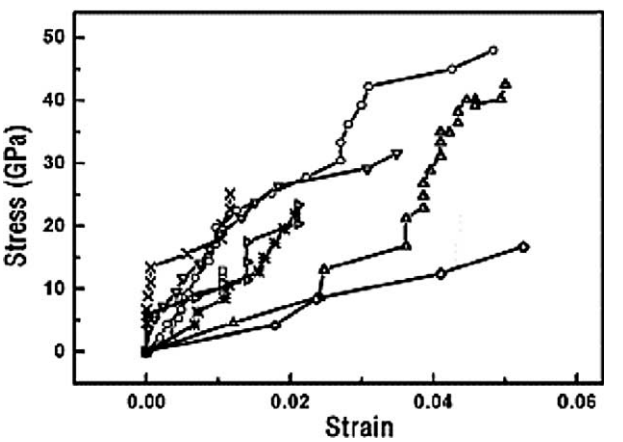

Fig. 5. Eight stress versus strain curves obtained from the tensile-loading experiments on individual SWCNT bundles. The values of the nominal stress are calculated using the cross-sectional area of the perimeter SWCNTs assuming a thickness of 0.34 nm. The strain is the engineering strain (from [55], with permission of the American Physical Society).

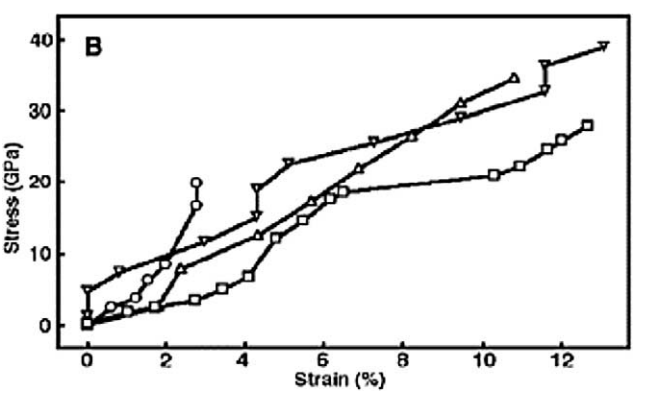

Fig. 6. Plot of stress versus strain curves for 5 individual MWCNTs. (Reprinted with permission from [56]. Copyright 2000 American Association for the Advancement of Science.)

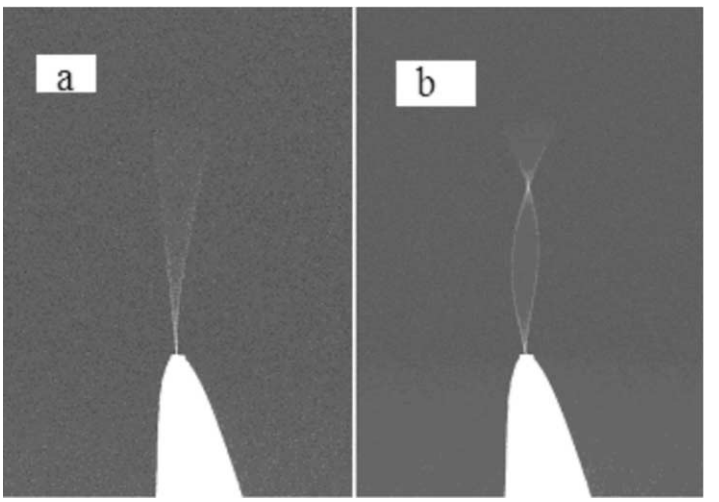

Fig. 7. Scanning electron microscope (SEM) images of electric field induced resonance of an individual MWCNT at: (a) its fundamental resonance frequency; and (b) its second order harmonic.

values were reported as ranging from 0.4 to 4.15 TPa with a mean of 1.8 TPa. A similar experimental study on SWCNT was presented by Krishnan et al. [61], who reported an average Young's modulus of 1.3–0.4/+0.6 TPa from measured amplitudes of 27 SWCNTs. Using the same structural model, Poncharal et al. [62] measured the resonance frequency of MWCNTs by driving the resonance with a counter electrode and RF excitation. They obtained Young's modulus of approximately 1 TPa for MWCNT with radius smaller than 12 nm; when the resonance response was fit by the assumption of a homogeneous resonating beam for larger diameter MWCNTs, a sharp drop in Young's modulus was fit. The authors attribute this to the occurrence of a rippling pattern and its influence on the resonance behaviour of the larger diameter MWCNTs; they and others have observed 'ring-pattern buckling' in compressively loaded MWCNTs. A similar type of experiment has also recently been realized by Yu et al. [63] and Dikin et al. [64] inside a scanning electron microscope (SEM) (Fig. 7).

A theoretical evaluation of Young's modulus can be obtained either by directly computing the mechanical response or by deriving it analytically. Overney et al. [65] calculated Young's modulus using an empirical Keating Hamiltonian with parameters determined from first principles in the computation. Their calculation, as pointed out by Treacy et al. [60], implies a Young's modulus ranging from 1.5 to 5.0 TPa. The Young's modulus can also be estimated by evaluating the energy in the CNT system. The relation that the strain energy of the tube is proportional to $1/R^2$ (where R is the radius of the CNT) was reported in the energetics analysis of Tibbetts [66], Robertson et al. [29], and Gao et al. [67]. Gao et al. [67] obtained values of Young's modulus from 640.30 GPa to 673.49 GPa by computing the second derivative of the potential energy. Yakobson et al. [68] fitted results from molecular dynamics (MD) simulations to the continuum shell model [69]. Unlike the previous work that assumes a thickness of 0.34 nm, both the thickness *and* Young's modulus were taken as the fitting parameters, yielding a thickness of 0.066 nm and Young's modulus of ∼5.5 TPa. The MD approach was also used by Lu [70] and he reported a Young's modulus of ∼1 TPa, a shear modulus of ∼0.5 TPa, and also that chirality, radius and the number of walls have little effect on the value of Young's modulus. A different potential model was used by Yao et al. [71] who obtained 1 TPa. Based on a nonorthogonal tight-binding scheme, Hernandez et al. [72] computed a 'surface Young's modulus' of 0.42 TPa-nm, yielding a Young's modulus of 1.2 TPa if one assumes the thickness of 0.34 nm for comparison to the in-plane compliances of graphite. Using the electronic band theory, Zhou et al. [73] obtained a Young's modulus of 5.1 TPa for an effective wall thickness of 0.71 Å for SWCNT.

The elastic properties were also discussed in the theoretical analysis by Govinjee and Sackman [74] based on Euler beam theory. They showed the size dependency of the elastic properties at the nanoscale, which does not occur at continuum scale. Harik further proposed [75,76] three non-dimensional parameters to validate the beam assumption. A shell model was used by Ru [77–82] to examine the effects of interlayer forces on the buckling and bending of CNTs; these approaches may be helpful for analyzing CNT embedded in an elastic matrix [80,81].

4.2. Application of crystal elasticity theory

The drawback of fitting the elastic constants based on a particular structural model is obvious: these constants are fitted based on assumptions that may not be correct. For instance, some elastic constants are obtained based on the assumption that CNT can be modeled as an isotropic elastic material, while it is not clear under what condition this assumption is going to be

valid. A mechanism-based approach that has a consistent link between the atomic structure and its continuum property is the *crystal elasticity approach*.

In the framework of finite strain, the relation between each elastic constant and a certain measure of deformation can be derived. For instance, if the energy density W of the material and Green–Lagrangian strain $\boldsymbol{E}$ is known, then the so-called second elasticity tensor is given as [83]

$$\boldsymbol{C}^{\mathrm{SE}} = \frac{\partial^2 W}{\partial \boldsymbol{E} \partial \boldsymbol{E}} \quad \text{or} \quad C^{\mathrm{SE}}_{ijkl} = \frac{\partial^2 W}{\partial E_{ij} \partial E_{kl}}. \tag{4}$$

Here $\boldsymbol{E} = 1/2(\boldsymbol{F}^{\mathrm{T}}\boldsymbol{F} - \boldsymbol{I})$ and the deformation gradient $\boldsymbol{F}$ is defined as $F_{\mathrm{ij}} = \partial x_i / \partial X_j$; x and X are respectively the spatial and material coordinates and subscripts refer to the dimension. The link to the atomic potential is through the energy density W.

Eq. (4) implies the application of the Cauchy–Born rule [84–86], which assumes that the deformation is homogeneous in a local environment. However, it was pointed out by Cousins [87] that when the Bravais lattice is not axi-symmetric, an 'inner-displacement' exists on top of the homogeneity. The continuum framework that accounts for such an effect was considered in the work of Zhang et al. [88,89] and the computational framework of Arroyo and Belytschko [90]. The modified Cauchy–Born rule is now expressed as:

$$\boldsymbol{C}^{\mathrm{SE}} = \frac{\partial^2 \phi}{\partial \boldsymbol{E} \partial \boldsymbol{E}} + \frac{\partial^2 \phi}{\partial \boldsymbol{E} \partial (\Delta \boldsymbol{\eta})} \frac{\partial (\Delta \boldsymbol{\eta})}{\partial \boldsymbol{E}} \tag{5}$$

in which the term $\partial(\Delta\boldsymbol{\eta})/\partial\boldsymbol{E}$ is obtained by

$$\frac{\partial^2 \phi}{\partial \boldsymbol{E} \partial (\Delta \boldsymbol{\eta})} + \frac{\partial^2 \phi}{\partial (\Delta \boldsymbol{\eta}) \partial (\Delta \boldsymbol{\eta})} \frac{\partial (\Delta \boldsymbol{\eta})}{\partial \boldsymbol{E}} = 0, \tag{6}$$

which leads to

$$\frac{\partial (\Delta \boldsymbol{\eta})}{\partial \boldsymbol{E}} = -\left[\frac{\partial^2 \phi}{\partial (\Delta \boldsymbol{\eta}) \partial (\Delta \boldsymbol{\eta})}\right]^{-1} \left(\frac{\partial^2 \phi}{\partial \boldsymbol{E} \partial (\Delta \boldsymbol{\eta})}\right). \tag{7}$$

The elastic modulus can therefore be evaluated as

$$\boldsymbol{C}^{\mathrm{SE}} = \left[\frac{\partial^2 \phi}{\partial \boldsymbol{E} \partial \boldsymbol{E}} + \frac{\partial^2 \phi}{\partial \boldsymbol{E} \partial (\Delta \boldsymbol{\eta})} \frac{\partial (\Delta \boldsymbol{\eta})}{\partial \boldsymbol{E}}\right]_{\boldsymbol{E}=0,\ \Delta\boldsymbol{\eta}=0}. \tag{8}$$

An important effect not considered in Eq. (8) is the effect of structural relaxation due to the curvature. As described in Section 2.2, the nanotube structure is that of a rolled graphene sheet. This is shown in Fig. 8. From Eq. (8), it can be seen that what was assumed in this procedure is that when the sheet is rolled into a tube, the bond length is unchanged; the rolled configuration (Fig. 8) is taken as the initial equilibrium configuration for the tube. Of course this is not true, particularly for nanotubes with small radius. The changes in bond length due to structural relaxation can be quite significant if the radius of the tube is small which will mean that the relaxed configuration differs from simply rolling the graphene sheet. The Young's modulus should be defined corresponding to this relaxed configuration, i.e.,

$$\boldsymbol{C}^{\mathrm{SE}} = \left[\frac{\partial^2 \phi}{\partial \boldsymbol{E} \partial \boldsymbol{E}} + \frac{\partial^2 \phi}{\partial \boldsymbol{E} \partial (\Delta \boldsymbol{\eta})} \frac{\partial (\Delta \boldsymbol{\eta})}{\partial \boldsymbol{E}}\right]_{\boldsymbol{E}=E_{\mathrm{relax}},\ \Delta\boldsymbol{\eta}=\Delta\eta_{\mathrm{relax}}}. \tag{9}$$

A detailed implementation can be found in [91].

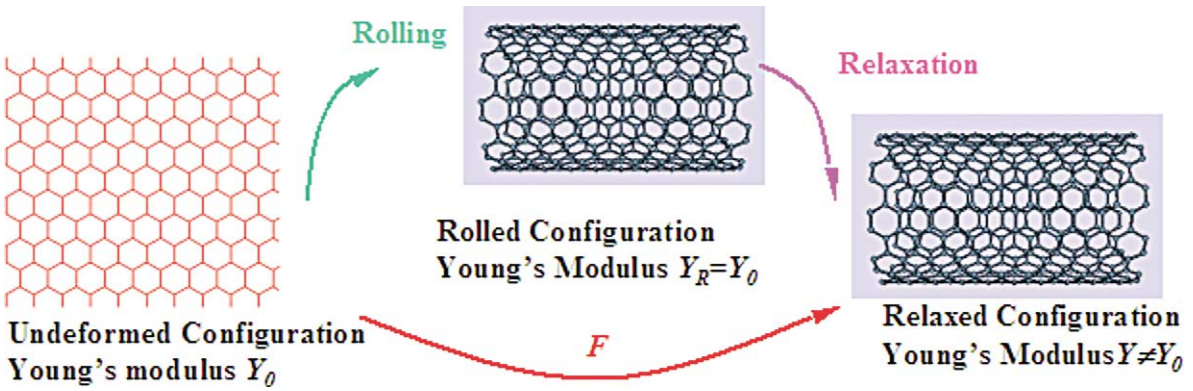

Fig. 8. Configurations involved in the structural relaxation of Carbon nanotubes.

5. Structural instability in CNT

The high aspect ratio in the CNT structure means they are susceptible to structural instability. A numerical study was conducted by Yakobson et al. [68,92] based on the Tersoff–Brenner potential. For the compressive loading case, a buckling strain of 0.05 was reported, followed by three subsequent buckles upon further loading. Buckling due to bending and torsion was demonstrated in [68,93–96], and is characterized by a collapse in the cross-section which results in a kink or ribbon-like structure.

Experimental observations of buckling in CNT were made by Despres et al. [97], Iijima et al. [98] and Ruoff et al. [99,100] using high resolution TEM (HRTEM) and Wong et al. [57] using AFM. AFM was used as a loading tool to bend MWCNT in the experiment by Falvo et al. [101] and Hertel et al. [102]. Lourie et al. [103] embedded CNT into a polymer film and were able to apply both compression and bending. Local rippling was observed in the buckled regions.

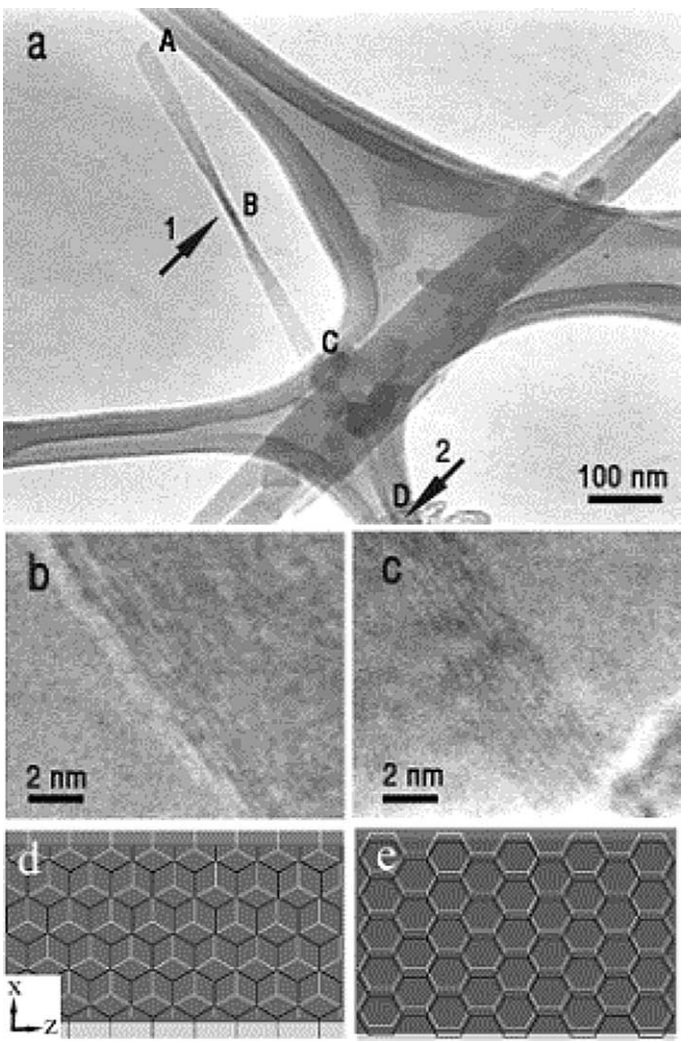

Fig. 9. A freestanding twisted MWCNT ribbon. (a) A TEM image of this ribbon anchored on one end by a carbon support film on a lacy carbon grid, but *unanchored* at the other end. Arrows point to the twists in the ribbon; (b) and (c) 8 resolved fringes along both edges of the ribbon imaged near the anchor point; (d) a schematic depicting the AB stacking between armchair CNT shells (the two layers are: the layer having brighter background and black lattices versus the layer having darker background and white lattices). The AB stacking can be achieved by just shifting the layer positions along the x direction that is perpendicular to the long axis of the MWCNT; (e) a schematic depicting the lattice alignment between the zigzag CNT shells by allowing the relative shifting of the layers along x direction. The AB stacking is not possible and only AA stacking or other stacking (as shown in the schematic) is possible (from [53], with permission of the American Physical Society).

A major factor that contributes to the buckling mode is the radial deformability of the tubes. Ruoff et al. [104] experimentally studied a system of two MWCNT adjacent to each other and concluded that CNTs in anisotropic physical environments (on a surface, near other objects such as other NTs) are not perfectly cylindrical; this arises due to the van der Waals attraction that develops an interfacial region much like the adhesion layer in biological vesicles. A closest-packed SWCNT crystal was further studied by Tersoff and Ruoff [105]. They found that tubes with diameters smaller than 1 nm are little affected (in their geometry) by the inter-tube interaction, but that tubes with diameter exceeding roughly 2.5 nm are obviously 'faceted'. Polygonized SWCNTs in contact have been reported by Lopez et al. [106].

Fully collapsed MWCNTs were observed in HRTEM by Chopra et al. [107] and Benedicts et al. [108]. Hertel et al. [109] and Avouris et al. [110] studied the radial deformation of MWCNTs on a substrate by both experiment (using AFM) and simulation; validating the prediction by Tersoff and Ruoff [105]. Fully or partially collapsed MWCNTs on surfaces have also been reported by Yu et al. [111,112], which also included an energetics analysis of the contact. The simulation by Lordi and Yao [113] indicated that the radial deformation can be reversible and elastic, depending on the type of CNT. Based on a MD-based energetic analysis, Gao et al. [67] studied the dependence of cross-sectional shape on the isolated SWCNT diameter. They found that the essentially circular shape is the stable cross-sectional shape if the radius of CNT is less than 1 nm, between 1 and 2 nm, both near-circular and collapsed shapes are favored, and that SWCNT should collapse to a ribbon for radius values larger than 3 nm.

One way to characterize the radial deformation is to perform a nano-identation test as reported by Shen et al. [114] using contact mode AFM. A deformability (up to 46%) of the tube and resilience to a significant compressive load (20 μN) was reported. A similar experiment was done by Yu et al. [115], who used AFM in tapping-mode. The elastic constant corresponding to the radial deformation was found to range from 0.3 GPa to 4 GPa based on a Hertzian contact model. A radial deformability of CNT under pressure was studied by Chesnokov et al. [116]; a volume compressibility of 0.0277 GPa^{-1} was measured, smaller than that of graphite (0.028 GPa^{-1}) [117]. The polygonization process of SWCNT bundles outlined above, but generated under high pressure, was also observed by Tang et al. [118–120]. They reported a compressibility of 0.024 GPa^{-1}.

When a CNT completely collapses to a ribbon, the interlayer interaction is analogous to that of two stacked graphene sheets. Due to the subtle change in the interlayer registration between two surfaces, a meta-stable configuration might exist. This was shown in the work by Yu et al. [53] (Fig. 9) who provided a simple energetics analysis demonstrating the presence of an energy barrier that prevent the twisted MWCNT ribbon from untwisting.

In short, the low dimensional geometry makes structural instability an important issue for the mechanical application of CNTs. Further study is needed for understanding mechanics in partially or fully collapsed CNT and CNT bundles.

6. Strength of nanotube and nanotube structures

6.1. Strength of CNT

The dramatic reduction in the length scale from the bulk material could result in an almost defect-free structure for nanostructures like CNT; if defect-free, the strength of CNT would be at the theoretical limit. The nature of the defect is closely related to the synthesis process. Arc-generation [121–123], laser ablation [124,125] and chemical vapor deposition (CVD) [126–128] are the three major synthesis methods. The distribution and types of defects in CNT will play a central role in their mechanical strength, and can also influence electrical and thermal transport; as such it is a topic deserving of further study.

Measuring the tensile strength of CNTs is an extremely challenging task. Tensile load testing was performed by Yu et al. [55] on SWCNT bundles and tensile strength values ranging from 13 to 52 GPa were reported; shown in Fig. 10 is an example of a SWCNT bundle that is being loaded and the maximum tensile strain obtained was 5.3%, which is close to the prediction by Nardelli et al. [129]. Yu et al. [56] have also conducted tensile testing of MWCNTs. It was found that only the outermost layer breaks during the loading process (Fig. 11). The tensile strength corresponding to this layer of CNT ranges from 11 to 63 GPa. By using AFM in a lateral force mode, an indirect measurement was done by Walters et al. [130]; a tensile strength of 45 ± 7 GPa was obtained using an assumed value for Young's modulus of 1.25 TPa for SWCNT. Long ropes ($\sim$2 mm in length) of aligned MWCNTs synthesized by the CVD method were tested by Pan et al. [131], and a much lower value of tensile strength was reported (1.72 ± 0.64 GPa).

To avoid the difficulties associated with direct tensile loading, indirect approaches have also been used. One method is to transfer the load to the CNT through a matrix material. Using this method, Wagner et al. [132] were able to fragment embedded SWCNT and a tensile strength of 55 GPa was reported. Similar work was done by Li et al. [133] and an average strength of $\sim$22 GPa was reported. Compressive loading of MWCNTs was reported by Lourie et al. [103], in which the compressive strength of 100–150 GPa and compressive strain of 5% were obtained.

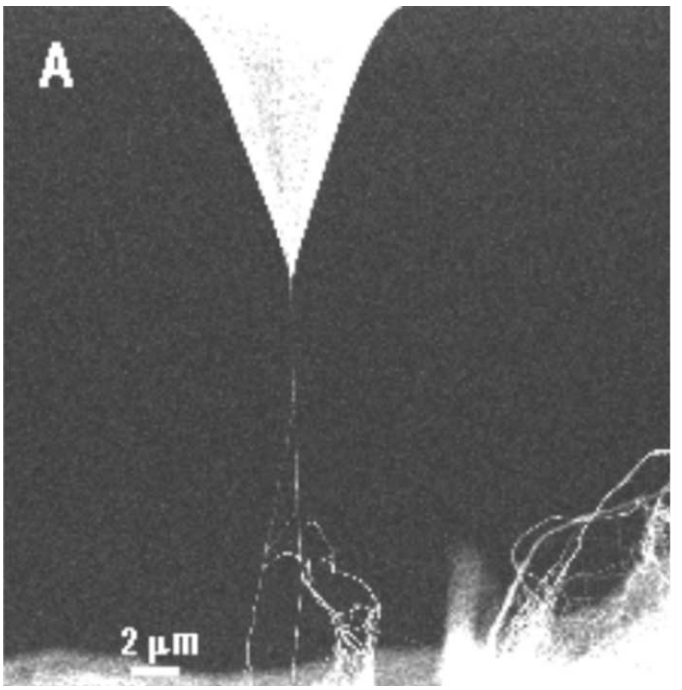

Fig. 10. SEM image of a tensile loaded SWCNT bundle between an AFM tip and a SWCNT "buckytube *paper*" sample (from [55], with permission of the American Physical Society).

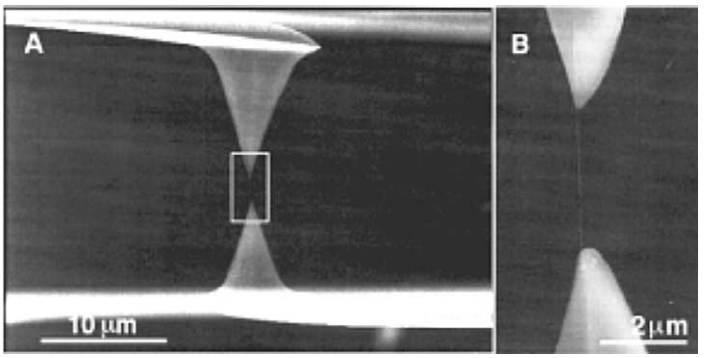

Fig. 11. Tensile loading of individual MWCNTs. (A) An SEM image of a MWCNT attached between two AFM tips; (B) higher magnification image of the indicated region in (A) showing the MWCNT between the AFM tips. (Reprinted with permission from [56]. Copyright 2000 American Association for the Advancement of Science.)

Compared with experiment, it is currently easier to model or compute the effects such as defects, loading rate, and temperature, have on the strength of CNT; of course the results obtained are model dependent. Yakobson et al. [68,92,93, 134] reported a tensile strain of 30% and strength of 150 GPa from a set of MD simulations. Belytschko et al. [135] reported a moderate dependence of fracture strength on chirality, based on MD simulation. The fracture strength was found to range between 93.5 GPa and 112 GPa and fracture strain was found to range between 15.8% and 18.7%.

A defect of particular significance is the pentagon/heptagon (or 5/7) defect (see Fig. 12, where the *Stone–Wales bond-rotation* [5] yields the '5–7–7–5 defect'. Based on their MD and quantum molecular dynamics (QMD) study, Nardelli et al. [136] found that such defects are energetically favored in otherwise defect-free armchair tubes when the tensile strain is greater than 5%; the rate of defect formation is, of course, a function of the temperature. When the QMD was run at temperatures higher than 2000 K, plastic flow was observed for a subset of CNT types. The compressive behavior was studied by Srivastava et al. [137] and the strength obtained is approximately 153 GPa. Strain rate effect is studied in the work of Wei et al. [138] and Srivastava et al. [139], in which they primarily focused on the compressive behavior as well. Local formation of sp^3 bonds

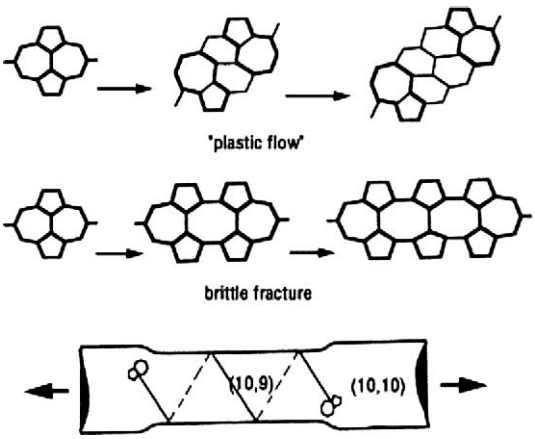

Fig. 12. The '5–7–7–5' dislocation further evolves as either a crack (brittle cleavage), or as a pair of dislocations gliding away along the spiral 'slip plane' (plastic yield). In the latter case, the change of the nanotube chirality is reflected by a stepwise change of diameter and by corresponding variations of electrical properties. (Reprinted from [143], with permission from Elsevier Science.)

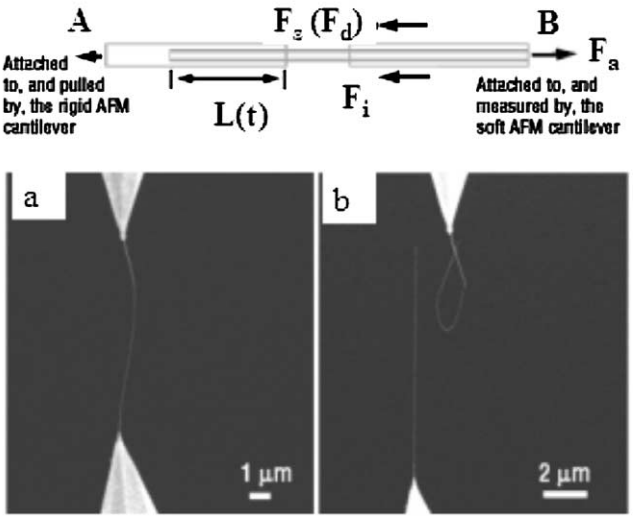

Fig. 13. The forces involved in the shell-sliding experiment can be described by $F_a = F_s + F_i = \pi\, d\tau\, L(t) + F_i$, where F_a is the applied pulling force as a function of time, τ is the shear strength, L is the contact length, d the shell diameter, and F_i is a diameter dependent force originating from both surface tension and 'edge effects'. SEM images showing the sword-in-sheath breaking mechanism of MWCNTs: (a) a MWCNT attached between AFM tips under no tensile load; (b) the same MWCNT after being tensile loaded to break. Notice the apparent overall length change of the MWCNT fragments after break compared to the initial length and the curling of the top MWCNT fragment in (b). (Reproduced with permission from [146]. Copyright 2000 Am. Chem. Soc.)

and development of 5/7 defects were reported. Yakobson [93,140] found that the formation of 5/7 defects is dependent on the chirality; defect nucleation is less favored in zig zag versus armchair tubes. The effect of plastic yielding on the electronic structure has been studied by Zhang et al. [141], in which a transition from metallic to semiconducting behaviour is reported. Zhang et al. [141] also observed a strong dependence of elastic limit on the chirality; with the same radius, an $(n, 0)$ tube can have twice the elastic limit of an (n, n) tube, and the compressive strength was found to range from 100 to 170 GPa. A different defect formation mechanism was described by Zhang and Crespi [142], which is characterized by spontaneous opening of double-layered graphitic patches in SWCNT.

6.2. Strength of CNT structures

The current synthesized CNTs are not individual SWCNT or MWCNTs. The primary product is typically either randomly agglomerated MWCNTs or SWCNT bundles [124,144]. It is important to note that the high stiffness and high strength properties of individual SWCNT do not necessarily imply the same properties in CNT structures.

Tensile loading of individual MWCNTs was presented by Yu et al. [56] who showed that only the outermost layer of MWCNT was able to be loaded (for the clamping method used) and the load transfer to the inner layers of MWCNT was observed to be very weak. The measured shear strength was only 0.08 MPa and 0.3 MPa (Fig. 13) for measurements of shell sliding in two separate MWCNTs. The weak load transfer was also demonstrated by Cumings and Zettl [145], who modeled a shear strength of 0.66 and 0.43 MPa as an explanation of shell-sliding observed in a TEM.

For SWCNT bundles, the tensile response of these has been measured by Yu et al. [55]. The weak inter-tube interaction can be estimated for a simple case of SWCNT bundle in parallel. As estimated by Qian et al. [147], the necessary contact length to achieve a good load transfer must be $\sim$1.3 μm. A possible way of enhancing the load transfer is that one can introduce twist to the system and make a nanorope. The detailed analysis of such structure is presented by Qian et al. [147], who drew inspiration from textile and twisted metal wire continuum mechanics. Recently, progress has been made in terms of the surface modification of CNT structures [148] and how this changes the structural properties of CNT needs further study.

7. Conclusions

The mechanical properties of CNTs and related structures were briefly reviewed. Our emphasis has been on elastic properties, deformability including buckling, twisting, and flattening, and inelastic behavior such as fracture and plastic yielding. Both experiment and theory/modeling were discussed.

Even though the mechanical properties of CNTs have been extensively studied, it is also fair to say that the very tip of the iceberg has been, so to speak, addressed. The challenge remains of establishing a data base of mechanical properties of CNTs as a function of concentration and type of defects, temperature, chemical environment, presence of chemical functionality, cycling of load, lifetime, and so on. The importance, due to the high expected strength, the known high stiffness in tensile load, and the low density, of CNT materials means that their mechanical properties deserve and will surely receive scrutiny for decades to come.

Acknowledgements

QD acknowledges the support of this work from the Ohio Board of Regents. RSR appreciates support from the NASA Langley Research Center Computational Materials: Nanotechnology Modeling and Simulation Program, from the NASA University Research, Engineering and Technology Institute on Bio Inspired Materials under award No. NCC-1-02037, the Office of Naval Research through contract N000140210870 (“Mechanics of Nanostructures”) and for support to RSR and WKL through the NSF grant “Mechanics of Nanoropes” (Ken Chong and Oscar Dillon, program managers).

References

[1] A.A. Mamedv, N.A. Kotov, M. Prato, D.M. Guldi, J.P. Wicksted, A. Hirsch, Molecular design of strong single-wall carbon nanotube/polyelectrolyte multilayer composites, Nature Materials 1 (2002) 190–194.
[2] T.L.L. Brown, B.E. Bursten, H.E. Lemay, Chemistry: The Central Science, 8th edition, Prentice-Hall, 1999.
[3] M. Fujita, R. Saito, G. Dresselhaus, M.S. Dresselhaus, Formation of general fullerenes by their projection on a honeycomb lattice, Phys. Rev. B 45 (23) (1992) 13834–13836.
[4] M.S. Dresselhaus, G. Dresselhaus, R. Saito, Physics of carbon nanotubes, Carbon 33 (7) (1995) 883–891.
[5] M.S. Dresselhaus, G. Dresselhaus, P.C. Eklund, Science of Fullerenes and Carbon Nanotubes, Academic Press, San Diego, 1996.
[6] M.S. Dresselhaus, G. Dresselhaus, P.C. Eklund, Fullerenes, J. Mater. Res. 8 (1993) 2054.
[7] S. Iijima, T. Ichihashi, Y. Ando, Pentagons, heptagons and negative curvature in graphite microtubule growth, Nature 356 (6372) (1992) 776–778.
[8] S. Iijima, Growth of carbon nanotubes, Mater. Sci. Engrg. B 19 (1–2) (1993) 172–180.
[9] Y. Saito, T. Yoshikawa, S. Bandow, M. Tomita, T. Hayashi, Interlayer spacings in carbon nanotubes, Phys. Rev. B 48 (3) (1993) 1907–1909.
[10] O. Zhou, R.M. Fleming, D.W. Murphy, C.H. Chen, R.C. Haddon, A.P. Ramirez, S.H. Glarum, Defects in carbon nanostructures, Science 263 (5154) (1994) 1744–1747.

[11] C.H. Kiang, M. Endo, P.M. Ajayan, G. Dresselhaus, M.S. Dresselhaus, Size effects in carbon nanotubes, Phys. Rev. Lett. 81 (9) (1998) 1869–1872.
[12] S. Amelinckx, D. Bernaerts, X.B. Zhang, G. Vantendeloo, J. Vanlanduyt, A structure model and growth-mechanism for multishell carbon nanotubes, Science 267 (5202) (1995) 1334–1338.
[13] J.G. Lavin, S. Subramoney, R.S. Ruoff, S. Berber, D. Tomanek, Scrolls and nested tubes in multiwall carbon tubes, Carbon 40 (7) (2001) 1123–1130.
[14] P.M. Ajayan, T.W. Ebbesen, Nanometre-size tubes of carbon, Rep. Progr. Phys. 60 (10) (1997) 1025–1062.
[15] N.L. Allinger, Conformational-analysis. 130. Mm2 – hydrocarbon force-field utilizing V1 and V2 torsional terms, J. Am. Chem. Soc. 99 (25) (1977) 8127–8134.
[16] N.L. Allinger, Y.H. Yuh, J.H. Lii, Molecular mechanics – the Mm3 force-field for hydrocarbons. 1, J. Am. Chem. Soc. 111 (23) (1989) 8551–8566.
[17] S.L. Mayo, B.D. Olafson, W.A. Goddard, Dreiding – a generic force-field for molecular simulations, J. Phys. Chem. 94 (26) (1990) 8897–8909.
[18] Y.J. Guo, N. Karasawa, W.A. Goddard, Prediction of fullerene packing in C60 and C70 crystals, Nature 351 (6326) (1991) 464–467.
[19] R.E. Tuzun, D.W. Noid, B.G. Sumpter, R.C. Merkle, Dynamics of fluid flow inside carbon nanotubes, Nanotechnology 7 (3) (1996) 241–246.
[20] R.E. Tuzun, D.W. Noid, B.G. Sumpter, R.C. Merkle, Dynamics of He/C-60 flow inside carbon nanotubes, Nanotechnology 8 (3) (1997) 112–118.
[21] G.C. Abell, Empirical chemical pseudopotential theory of molecular and metallic bonding, Phys. Rev. B 31 (10) (1985) 6184–6196.
[22] J. Tersoff, New empirical-model for the structural-properties of silicon, Phys. Rev. Lett. 56 (6) (1986) 632–635.
[23] J. Tersoff, New empirical-approach for the structure and energy of covalent systems, Phys. Rev. B 37 (12) (1988) 6991–7000.
[24] J. Tersoff, Empirical interatomic potential for carbon, with applications to amorphous-carbon, Phys. Rev. Lett. 61 (25) (1988) 2879–2882.
[25] J. Tersoff, Modeling solid-state chemistry – interatomic potentials for multicomponent systems, Phys. Rev. B 39 (8) (1989) 5566–5568.
[26] D.W. Brenner, Empirical potential for hydrocarbons for use in simulating the chemical vapor-deposition of diamond films, Phys. Rev. B 42 (15) (1990) 9458–9471.
[27] D.W. Brenner, J.A. Harrison, C.T. White, R.J. Colton, Molecular-dynamics simulations of the nanometer-scale mechanical-properties of compressed buckminsterfullerene, Thin Solid Films 206 (1–2) (1991) 220–223.
[28] D.H. Robertson, D.W. Brenner, C.T. White, On the way to fullerenes – molecular-dynamics study of the curling and closure of graphitic ribbons, J. Phys. Chem. 96 (15) (1992) 6133–6135.
[29] D.H. Robertson, D.W. Brenner, J.W. Mintmire, Energetics of nanoscale graphitic tubules, Phys. Rev. B 45 (21) (1992) 12592–12595.
[30] D.H. Robertson, D.W. Brenner, C.T. White, Temperature-dependent fusion of colliding C-60 fullerenes from molecular-dynamics simulations, J. Phys. Chem. 99 (43) (1995) 15721–15724.
[31] J.A. Harrison, C.T. White, R.J. Colton, D.W. Brenner, Nanoscale investigation of indentation, adhesion and fracture of diamond (111) surfaces, Surface Sci. 271 (1–2) (1992) 57–67.
[32] J.A. Harrison, C.T. White, R.J. Colton, D.W. Brenner, Molecular-dynamics simulations of atomic-scale friction of diamond surfaces, Phys. Rev. B 46 (15) (1992) 9700–9708.
[33] J.A. Harrison, R.J. Colton, C.T. White, D.W. Brenner, Effect of atomic-scale surface-roughness on friction – a molecular-dynamics study of diamond surfaces, Wear 168 (1–2) (1993) 127–133.
[34] J.A. Harrison, C.T. White, R.J. Colton, D.W. Brenner, Effects of chemically-bound, flexible hydrocarbon species on the frictional-properties of diamond surfaces, J. Phys. Chem. 97 (25) (1993) 6573–6576.
[35] J.A. Harrison, C.T. White, R.J. Colton, D.W. Brenner, Atomistic simulations of friction at sliding diamond interfaces, Mrs Bulletin 18 (5) (1993) 50–53.
[36] J.A. Harrison, D.W. Brenner, Simulated tribochemistry – an atomic-scale view of the wear of diamond, J. Am. Chem. Soc. 116 (23) (1994) 10399–10402.
[37] J.A. Harrison, C.T. White, R.J. Colton, D.W. Brenner, Investigation of the atomic-scale friction and energy-dissipation in diamond using molecular-dynamics, Thin Solid Films 260 (2) (1995) 205–211.
[38] K.J. Tupper, D.W. Brenner, Atomistic simulations of frictional wear in self-assembled monolayers, Abstr. Papers Am. Chem. Soc. 206 (1993) 172-POLY.
[39] K.J. Tupper, D.W. Brenner, Molecular-dynamics simulations of interfacial dynamics in self-assembled monolayers, Abstr. Papers Am. Chem. Soc. 206 (1993) 72-COMP.
[40] K.J. Tupper, D.W. Brenner, Molecular-dynamics simulations of friction in self-assembled monolayers, Thin Solid Films 253 (1–2) (1994) 185–189.
[41] D.W. Brenner, 2001, unpublished.
[42] D.W. Brenner, The art and science of an analytic potential, Phys. Status Solidi B 217 (1) (2000) 23–40.
[43] D.G. Pettifor, Oleinik II, Analytic bond-order potentials beyond Tersoff–Brenner. II. Application to the hydrocarbons, Phys. Rev. B 59 (13) (1999) 8500.
[44] D.G. Pettifor, Oleinik II, Bounded analytic bond-order potentials for sigma and pi bonds, Phys. Rev. Lett. 84 (18) (2000) 4124–4127.
[45] L.A. Girifalco, R.A. Lad, Energy of cohesion, compressibility and the potential energy functions of the graphite system, J. Chem. Phys. 25 (4) (1956) 693–697.
[46] L.A. Girifalco, Molecular-properties of C-60 in the gas and solid-phases, J. Phys. Chem. 96 (2) (1992) 858–861.
[47] L.A. Girifalco, M. Hodak, R.S. Lee, Carbon nanotubes, buckyballs, ropes, and a universal graphitic potential, Phys. Rev. B 62 (19) (2000) 13104–13110.

[48] Y. Wang, D. Tomanek, G.F. Bertsch, Stiffness of a solid composed of C60 clusters, Phys. Rev. B 44 (12) (1991) 6562–6565.
[49] D. Qian, W.K. Liu, R.S. Ruoff, Mechanics of C60 in nanotubes, J. Phys. Chem. B 105 (2001) 10753–10758.
[50] M. Hanfland, H. Beister, K. Syassen, Graphite under pressure – equation of state and 1st-order Raman modes, Phys. Rev. B 39 (17) (1989) 12598–12603.
[51] J.C. Boettger, All-electron full-potential calculation of the electronic band structure, elastic constants, and equation of state for graphite, Phys. Rev. B 55 (17) (1997) 11202–11211.
[52] A.N. Kolmogorov, V.H. Crespi, Smoothest bearings: interlayer sliding in multiwalled carbon nanotubes, Phys. Rev. Lett. 85 (22) (2000) 4727–4730.
[53] M.F. Yu, M.J. Dyer, J. Chen, D. Qian, W.K. Liu, R.S. Ruoff, Locked twist in multi-walled carbon nanotube ribbons, Phys. Rev. B 64 (2001) 241403R.
[54] O. Lourie, H.D. Wagner, Evaluation of Young's modulus of carbon nanotubes by micro-Raman spectroscopy, J. Mater. Res. 13 (9) (1998) 2418–2422.
[55] M.F. Yu, B.S. Files, S. Arepalli, R.S. Ruoff, Tensile loading of ropes of single wall carbon nanotubes and their mechanical properties, Phys. Rev. Lett. 84 (24) (2000) 5552–5555.
[56] M.F. Yu, O. Lourie, M.J. Dyer, K. Moloni, T.F. Kelly, R.S. Ruoff, Strength and breaking mechanism of multiwalled carbon nanotubes under tensile load, Science 287 (5453) (2000) 637–640.
[57] E.W. Wong, P.E. Sheehan, C.M. Lieber, Nanobeam mechanics: elasticity, strength, and toughness of nanorods and nanotubes, Science 277 (5334) (1997) 1971–1975.
[58] J.P. Salvetat, A.J. Kulik, J.M. Bonard, G.A.D. Briggs, T. Stockli, K. Metenier, S. Bonnamy, F. Beguin, N.A. Burnham, L. Forro, Elastic modulus of ordered and disordered multiwalled carbon nanotubes, Adv. Mater. 11 (2) (1999) 161–165.
[59] J.P. Salvetat, G.A.D. Briggs, J.M. Bonard, R.R. Bacsa, A.J. Kulik, T. Stockli, N.A. Burnham, L. Forro, Elastic and shear moduli of single-walled carbon nanotube ropes, Phys. Rev. Lett. 82 (5) (1999) 944–947.
[60] M.M.J. Treacy, T.W. Ebbesen, J.M. Gibson, Exceptionally high Young's modulus observed for individual carbon nanotubes, Nature 381 (6584) (1996) 678–680.
[61] A. Krishnan, E. Dujardin, T.W. Ebbesen, P.N. Yianilos, M.M.J. Treacy, Young's modulus of single-walled nanotubes, Phys. Rev. B 58 (20) (1998) 14013–14019.
[62] P. Poncharal, Z.L. Wang, D. Ugarte, W.A. de Heer, Electrostatic deflections and electromechanical resonances of carbon nanotubes, Science 283 (5407) (1999) 1513–1516.
[63] M.F. Yu, M.J. Dyer, J. Chen, K. Bray, Multiprobe nanomanipulation and functional assembly of nanomaterials inside a scanning electron microscope, in: International Conference IEEE-NANO2001, Maui, 2001.
[64] D.A. Dikin, X. Chen, W. Ding, G.J. Wagner, R.S. Ruoff, Resonance vibration of amorphous SiO_2 nanowires driven by mechanical or electrical field excitation, J. Appl. Phys. 93 (2003) 226.
[65] G. Overney, W. Zhong, D. Tomanek, Structural rigidity and low-frequency vibrational-modes of long carbon tubules, Z. Phys. D 27 (1) (1993) 93–96.
[66] G.G. Tibbetts, Why are carbon filaments tubular, J. Crystal Growth 66 (3) (1984) 632–638.
[67] G.H. Gao, T. Cagin, W.A. Goddard, Energetics, structure, mechanical and vibrational properties of single-walled carbon nanotubes, Nanotechnology 9 (3) (1998) 184–191.
[68] B.I. Yakobson, C.J. Brabec, J. Bernholc, Nanomechanics of carbon tubes: Instabilities beyond linear response, Phys. Rev. Lett. 76 (14) (1996) 2511–2514.
[69] S. Timoshenko, J. Gere, Theory of of Elastic Stability, McGraw-Hill, New York, 1988.
[70] J.P. Lu, Elastic properties of carbon nanotubes and nanoropes, Phys. Rev. Lett. 79 (7) (1997) 1297–1300.
[71] N. Yao, V. Lordi, Young's modulus of single-walled carbon nanotubes, J. Appl. Phys. 84 (4) (1998) 1939–1943.
[72] E. Hernandez, C. Goze, P. Bernier, A. Rubio, Elastic properties of C and $BxCyNz$ composite nanotubes, Phys. Rev. Lett. 80 (20) (1998) 4502–4505.
[73] X. Zhou, J.J. Zhou, Z.C. Ou-Yang, Strain energy and Young's modulus of single-wall carbon nanotubes calculated from electronic energy-band theory, Phys. Rev. B 62 (20) (2000) 13692–13696.
[74] S. Govindjee, J.L. Sackman, On the use of continuum mechanics to estimate the properties of nanotubes, Solid State Commun. 110 (4) (1999) 227–230.
[75] V.M. Harik, Mechanics of carbon nanotubes: applicability of the continuum-beam models, Comput. Mater. Sci. 24 (3) (2002) 328–342.
[76] V.M. Harik, Ranges of applicability for the continuum-beam model in the mechanics of carbon-nanotubes and nanorods, Solid State Commun. 120 (331–335) (2001).
[77] C.Q. Ru, Effect of van der Waals forces on axial buckling of a double-walled carbon nanotube, J. Appl. Phys. 87 (10) (2000) 7227–7231.
[78] C.Q. Ru, Effective bending stiffness of carbon nanotubes, Phys. Rev. B 62 (15) (2000) 9973–9976.
[79] C.Q. Ru, Column buckling of multiwalled carbon nanotubes with interlayer radial displacements, Phys. Rev. B 62 (24) (2000) 16962–16967.
[80] C.Q. Ru, Degraded axial buckling strain of multiwalled carbon nanotubes due to interlayer slips, J. Appl. Phys. 89 (6) (2001) 3426–3433.
[81] C.Q. Ru, Axially compressed buckling of a doublewalled carbon nanotube embedded in an elastic medium, J. Mech. Phys. Solids 49 (6) (2001) 1265–1279.
[82] C.Q. Ru, Elastic buckling of single-walled carbon nanotube ropes under high pressure, Phys. Rev. B 62 (15) (2000) 10405–10408.
[83] T. Belytschko, W.K. Liu, B. Moran, Nonlinear Finite Elements for Continua and Structures, Wiley, 2000.
[84] E.B. Tadmor, M. Ortiz, R. Phillips, Quasicontinuum analysis of defects in solids, Philos. Mag. A 73 (6) (1996) 1529–1563.
[85] F. Milstein, Crystal elasticity, in: M.J. Sewell (Ed.), Mechanics of Solids, Pergamon Press, Oxford, 1982.

[86] J.L. Ericksen, in: M. Gurtin (Ed.), Phase Transformations and Material Instabilities in Solids, Academic Press, New York, 1984.
[87] C.S.G. Cousins, Inner elasticity, J. Phys. C 11 (24) (1978) 4867–4879.
[88] P. Zhang, Y. Huang, H. Gao, K.C. Hwang, Fracture nucleation in single-wall carbon nanotubes under tension: A continuum analysis incorporating interatomic potentials, J. Appl. Mech. 69 (4) (2002) 454–458.
[89] P. Zhang, Y. Huang, P.H. Geubelle, P. Klein, K.C. Hwang, The elastic modulus of single-wall carbon nanotubes: A continuum analysis incorporating interatomic potentials, Int. J. Solids Structures 39 (13–14) (2002) 3893–3906.
[90] M. Arroyo, T. Belytschko, An atomistic-based membrane for crystalline films one atom thick, J. Mech. Phys. Solids 50 (2002) 1941–1977.
[91] D. Qian, Effect of relaxation on the elastic properties of carbon nanotube, 2003, in preparation.
[92] B.I. Yakobson, R.E. Smalley, Fullerene nanotubes: C-1000000 and beyond, Am. Sci. 85 (4) (1997) 324–337.
[93] B.I. Yakobson, P. Avouris, Mechanical properties of carbon nanotubes, in: Carbon Nanotubes, 2001, pp. 287–327.
[94] J. Bernholc, C. Brabec, M.B. Nardelli, A. Maiti, C. Roland, B.I. Yakobson, Theory of growth and mechanical properties of nanotubes, Appl. Phys. A 67 (1) (1998) 39–46.
[95] D. Qian, W.K. Liu, R.S. Ruoff, Bent and kinked multi-shell Carbon nanotubes-treating the interlayer potential more realistically, in: 43rd AIAA/ASME/ASCE/AHS Structures, Structural Dynamics, and Materials Conferences, Denver, CO, 2002.
[96] D. Qian, W.K. Liu, S. Subramoney, R.S. Ruoff, Effect of interlayer interaction on the mechanical deformation of multiwalled carbon nanotube, J. Nanosci. Nanotechnol. 3 (1) (2003) 185–191.
[97] J.F. Despres, E. Daguerre, K. Lafdi, Flexibility of graphene layers in carbon nanotubes, Carbon 33 (1) (1995) 87–89.
[98] S. Iijima, C. Brabec, A. Maiti, J. Bernholc, Structural flexibility of carbon nanotubes, J. Chem. Phys. 104 (5) (1996) 2089–2092.
[99] R.S. Ruoff, D.C. Lorents, R. Laduca, S. Awadalla, S. Weathersby, K. Parvin, S. Subramoney, Proc. Electrochem. Soc. 95–10 (1995) 557–562.
[100] S. Subramoney, R.S. Ruoff, R. Laduca, S. Awadalla, K. Parvin, Proc. Electrochem. Soc. 95–10 (1995) 563–569.
[101] M.R. Falvo, G.J. Clary, R.M. Taylor, V. Chi, F.P. Brooks, S. Washburn, R. Superfine, Bending and buckling of carbon nanotubes under large strain, Nature 389 (6651) (1997) 582–584.
[102] T. Hertel, R. Martel, P. Avouris, Manipulation of individual carbon nanotubes and their interaction with surfaces, J. Phys. Chem. B 102 (6) (1998) 910–915.
[103] O. Lourie, D.M. Cox, H.D. Wagner, Buckling and collapse of embedded carbon nanotubes, Phys. Rev. Lett. 81 (8) (1998) 1638–1641.
[104] R.S. Ruoff, J. Tersoff, D.C. Lorents, S. Subramoney, B. Chan, Radial deformation of carbon nanotubes by Van-Der-Waals forces, Nature 364 (6437) (1993) 514–516.
[105] J. Tersoff, R.S. Ruoff, Structural-properties of a carbon-nanotube crystal, Phys. Rev. Lett. 73 (5) (1994) 676–679.
[106] M.J. Lopez, A. Rubio, J.A. Alonso, L.C. Qin, S. Iijima, Novel polygonized single-wall carbon nanotube bundles, Phys. Rev. Lett. 86 (14) (2001) 3056–3059.
[107] N.G. Chopra, L.X. Benedict, V.H. Crespi, M.L. Cohen, S.G. Louie, A. Zettl, Fully collapsed carbon nanotubes, Nature 377 (6545) (1995) 135–138.
[108] L.X. Benedict, N.G. Chopra, M.L. Cohen, A. Zettl, S.G. Louie, V.H. Crespi, Microscopic determination of the interlayer binding energy in graphite, Chem. Phys. Lett. 286 (5–6) (1998) 490–496.
[109] T. Hertel, R.E. Walkup, P. Avouris, Deformation of carbon nanotubes by surface van der Waals forces, Phys. Rev. B 58 (20) (1998) 13870–13873.
[110] P. Avouris, T. Hertel, R. Martel, T. Schmidt, H.R. Shea, R.E. Walkup, Carbon nanotubes: nanomechanics, manipulation, and electronic devices, Appl. Surface Sci. 141 (3–4) (1999) 201–209.
[111] M.F. Yu, M.J. Dyer, R.S. Ruoff, Structure and mechanical flexibility of carbon nanotube ribbons: An atomic-force microscopy study, J. Appl. Phys. 89 (8) (2001) 4554–4557.
[112] M.F. Yu, T. Kowalewski, R.S. Ruoff, Structural analysis of collapsed, and twisted and collapsed, multiwalled carbon nanotubes by atomic force microscopy, Phys. Rev. Lett. 86 (1) (2001) 87–90.
[113] V. Lordi, N. Yao, Radial compression and controlled cutting of carbon nanotubes, J. Chem. Phys. 109 (6) (1998) 2509–2512.
[114] W.D. Shen, B. Jiang, B.S. Han, S.S. Xie, Investigation of the radial compression of carbon nanotubes with a scanning probe microscope, Phys. Rev. Lett. 84 (16) (2000) 3634–3637.
[115] M.F. Yu, T. Kowalewski, R.S. Ruoff, Investigation of the radial deformability of individual carbon nanotubes under controlled indentation force, Phys. Rev. Lett. 85 (7) (2000) 1456–1459.
[116] S.A. Chesnokov, V.A. Nalimova, A.G. Rinzler, R.E. Smalley, J.E. Fischer, Mechanical energy storage in carbon nanotube springs, Phys. Rev. Lett. 82 (2) (1999) 343–346.
[117] B.T. Kelly, Physics of Graphite, Applied Science, London, 1981.
[118] J. Tang, L.C. Qin, T. Sasaki, M. Yudasaka, A. Matsushita, S. Iijima, Compressibility and polygonization of single-walled carbon nanotubes under hydrostatic pressure, Phys. Rev. Lett. 85 (9) (2000) 1887–1889.
[119] J. Tang, L.C. Qin, T. Sasaki, M. Yudasaka, A. Matsushita, S. Iijima, Structure and property changes of single-walled carbon nanotubes under pressure, Synthetic Metals 121 (1–3) (2001) 1245–1246.
[120] J. Tang, L.C. Qin, T. Sasaki, M. Yudasaka, A. Matsushita, S. Iijima, Revealing properties of single-walled carbon nanotubes under high pressure, J. Phys. Condensed Matter. 14 (44) (2002) 10575–10578.
[121] S. Iijima, Helical microtubules of graphitic carbon, Nature 354 (6348) (1991) 56–58.
[122] T.W. Ebbesen, P.M. Ajayan, Large-scale synthesis of carbon nanotubes, Nature 358 (6383) (1992) 220–222.
[123] S. Iijima, P.M. Ajayan, T. Ichihashi, Growth-model for carbon nanotubes, Phys. Rev. Lett. 69 (21) (1992) 3100–3103.

[124] A. Thess, R. Lee, P. Nikolaev, H.J. Dai, P. Petit, J. Robert, C.H. Xu, Y.H. Lee, S.G. Kim, A.G. Rinzler, D.T. Colbert, G.E. Scuseria, D. Tomanek, J.E. Fischer, R.E. Smalley, Crystalline ropes of metallic carbon nanotubes, Science 273 (5274) (1996) 483–487.
[125] T. Guo, P. Nikolaev, A. Thess, D.T. Colbert, R.E. Smalley, Catalytic growth of single-walled nanotubes by laser vaporization, Chem. Phys. Lett. 243 (1–2) (1995) 49–54.
[126] J. Kong, H.T. Soh, A.M. Cassell, C.F. Quate, H.J. Dai, Synthesis of individual single-walled carbon nanotubes on patterned silicon wafers, Nature 395 (6705) (1998) 878–881.
[127] A.M. Cassell, J.A. Raymakers, J. Kong, H.J. Dai, Large scale CVD synthesis of single-walled carbon nanotubes, J. Phys. Chem. B 103 (31) (1999) 6484–6492.
[128] W.Z. Li, S.S. Xie, L.X. Qian, B.H. Chang, B.S. Zou, W.Y. Zhou, R.A. Zhao, G. Wang, Large-scale synthesis of aligned carbon nanotubes, Science 274 (5293) (1996) 1701–1703.
[129] M.B. Nardelli, B.I. Yakobson, J. Bernholc, Brittle and ductile behavior in carbon nanotubes, Phys. Rev. Lett. 81 (21) (1998) 4656–4659.
[130] D.A. Walters, L.M. Ericson, M.J. Casavant, J. Liu, D.T. Colbert, K.A. Smith, R.E. Smalley, Elastic strain of freely suspended single-wall carbon nanotube ropes, Appl. Phys. Lett. 74 (25) (1999) 3803–3805.
[131] Z.W. Pan, S.S. Xie, L. Lu, B.H. Chang, L.F. Sun, W.Y. Zhou, G. Wang, D.L. Zhang, Tensile tests of ropes of very long aligned multiwall carbon nanotubes, Appl. Phys. Lett. 74 (21) (1999) 3152–3154.
[132] H.D. Wagner, O. Lourie, Y. Feldman, R. Tenne, Stress-induced fragmentation of multiwall carbon nanotubes in a polymer matrix, Appl. Phys. Lett. 72 (2) (1998) 188–190.
[133] F. Li, H.M. Cheng, S. Bai, G. Su, M.S. Dresselhaus, Tensile strength of single-walled carbon nanotubes directly measured from their macroscopic ropes, Appl. Phys. Lett. 77 (20) (2000) 3161–3163.
[134] B.I. Yakobson, M.P. Campbell, C.J. Brabec, J. Bernholc, High strain rate fracture and C-chain unraveling in carbon nanotubes, Comput. Mater. Sci. 8 (4) (1997) 341–348.
[135] T. Belytschko, S.P. Xiao, G.C. Schartz, R.S. Ruoff, Atomistic simulation of nanotube fracture, Phys. Rev. B 65 (235430) (2002).
[136] M.B. Nardelli, B.I. Yakobson, J. Bernholc, Mechanism of strain release in carbon nanotubes, Phys. Rev. B 57 (8) (1998) R4277–R4280.
[137] D. Srivastava, M. Menon, K.J. Cho, Nanoplasticity of single-wall carbon nanotubes under uniaxial compression, Phys. Rev. Lett. 83 (15) (1999) 2973–2976.
[138] C.Y. Wei, D. Srivastava, K.J. Cho, Molecular dynamics study of temperature dependent plastic collapse of carbon nanotubes under axial compression, Comput. Modeling Engrg. Sci. 3 (2002) 255.
[139] D. Srivastava, C.Y. Wei, K.J. Cho, Computational nanomechanics of carbon nanotubes and composites (submitted), ASME Appl. Mech. Rev. (2003).
[140] B.I. Yakobson, Mechanical relaxation and “intramolecular plasticity” in carbon nanotubes, Appl. Phys. Lett. 72 (8) (1998) 918–920.
[141] P.H. Zhang, P.E. Lammert, V.H. Crespi, Plastic deformations of carbon nanotubes, Phys. Rev. Lett. 81 (24) (1998) 5346–5349.
[142] P.H. Zhang, V.H. Crespi, Nucleation of carbon nanotubes without pentagonal rings, Phys. Rev. Lett. 83 (9) (1999) 1791–1794.
[143] B.I. Yakobson, Dynamic topology and yield strength of carbon nanotubes, in: Recent Advances in the Chemistry and Physics of Fullerenes and Related Materials, Electrochemical Society, Pennington, NJ, 1997.
[144] H.J. Dal, A.G. Rinzler, P. Nikolaev, A. Thess, D.T. Colbert, R.E. Smalley, Single-wall nanotubes produced by metal-catalyzed disproportionation of carbon monoxide, Chem. Phys. Lett. 260 (3–4) (1996) 471–475.
[145] J. Cumings, A. Zettl, Low-friction nanoscale linear bearing realized from multiwall carbon nanotubes, Science 289 (5479) (2000) 602–604.
[146] M.F. Yu, B.I. Yakobson, R.S. Ruoff, Controlled sliding and pullout of nested shells in individual multiwalled carbon nanotubes, J. Phys. Chem. B 104 (37) (2000) 8764–8767.
[147] D. Qian, W.K. Liu, R.S. Ruoff, Load transfer mechanism in carbon nanotube ropes, Composites Sci. Techn. 63 (11) (2003) 1561–1569.
[148] D. Shi, J. Lian, P. He, L.M. Wang, W.J.V. Oojj, M. Schulz, D. Mast, Plasma deposition of ultrathin polymer films on carbon nanotubes, Appl. Phys. Lett. 81 (27) (2002) 5216–5218.